coasts

MDPI

Article

Runoff and Sediment Flux on the North Coast of KwaZulu-Natal: Counter-Acting Beach Erosion from Rising Seas?

Mark R. Jury [1,2]

[1] Geography Department, University Zululand, KwaDlangezwa 3886, South Africa; mark.jury@upr.edu
[2] Physics Department, University Puerto Rico Mayaguez, Mayaguez, PR 00681, USA

Abstract

A remote analysis of coastal sedimentation in northern KwaZulu-Natal (KZN), South Africa, describes how summer runoff and winter wave-action operate within a highly variable climate. Despite rising sea levels, the sediment flux can sustain beaches under certain conditions. Daily satellite red-band reflectivity and ocean–atmosphere reanalysis datasets were studied over the period of 2018–2025. Statistical results indicate that streamflow discharges are spread northward by oblique wave-driven currents. Sediment concentrations peak during late winter (>1 mg/L, May–October) when deep turbulent mixing (>40 m) mobilizes sand from the seabed. A case study from September 2021 revealed that ridging high-pressure/cut-off low weather patterns can simultaneously increase streamflow, wave energy, and wind power, creating a surf-zone sediment conveyor along the coast of northern KZN. Long-term climate diagnostics from 1981 to 2025 reveal upward trends in coastal runoff, vegetation, and turbidity (0.29 σ/yr) that point to an increasingly vigorous water cycle. The warming of the southeast Atlantic intensifies the sub-tropical upper-level westerlies and late winter storms over southeast Africa. These processes occur in 5–8 year cycles and drive shoreline advance and retreat, from accretion ~1 T/m and storm surge inundations up to 5.5 m. Using Digital Earth, it was noted that ~1/4 of beaches around Africa are gaining sediment while ~1/3 are eroding. Although remote information could not close the sediment budget, realistic estimates of long-shore transport in the surf-zone (>10^4 kg/yr/m) and on the beach (>10^3 kg/yr/m) were calculated. These provide an emerging explanation for the resilience of northern KZN beaches, as sea levels rise at a rate of 0.6 cm/yr.

Keywords: beach sediment flux; erosion vs. runoff

Check for updates

Academic Editor: Bas W. Borsje

Received: 7 January 2026
Revised: 29 January 2026
Accepted: 4 March 2026
Published: 1 April 2026

Copyright: © 2026 by the author. Licensee MDPI, Basel, Switzerland. This article is an open access article distributed under the terms and conditions of the Creative Commons Attribution (CC BY) license.

1. Introduction

Coastlines are shaped by ancient geological history, fluctuating environmental conditions, and recent land use. A retreat of sandy beaches may be expected as seas rise in response to global warming [1–3], posing risks to the sustainability of coastal resources and ecotourism infrastructure. Vulnerability can be identified via digital elevation data, but the feedback between air–land–sea interactions is difficult to resolve via site-specific modeling [4].

As sediments delivered by catchment runoff reach the shore, oblique wave action generates turbulent long-shore currents that join tidal- and wind-driven flows to swash sand onto the beach [5–7]. Fluctuations in these environmental forces can lead to natural cycles of shoreline advance and retreat [8,9]. However, urban–industrial–agricultural land use often diverts sediment-laden streamflow [10] or inhibits downstream transport past

coastal infrastructure [11]. As global warming amplifies the risk of inundation [3,12,13], there is a need to monitor changes in the coastal sediment flux and trends in runoff and infiltration [14,15].

Northern KwaZulu-Natal (KZN, Figure 1a) is characterized by a relatively straight coastline, oriented 210–030°, backed by the Valley of a Thousand Hills, and incised by many rivers that tend to pulse in austral summer (December–March). The climate of southeast Africa is sub-tropical and humid due to the warm Agulhas Current and instability from passing atmospheric westerly waves undercut by easterly winds from the Mascarene High. Tropical cyclones are rare, but cut-off lows in spring and autumn can bring sporadic floods [16]. Big waves frequently sweep the coast during austral winter, driving northward surf-zone currents in a deep, mixed layer [17].

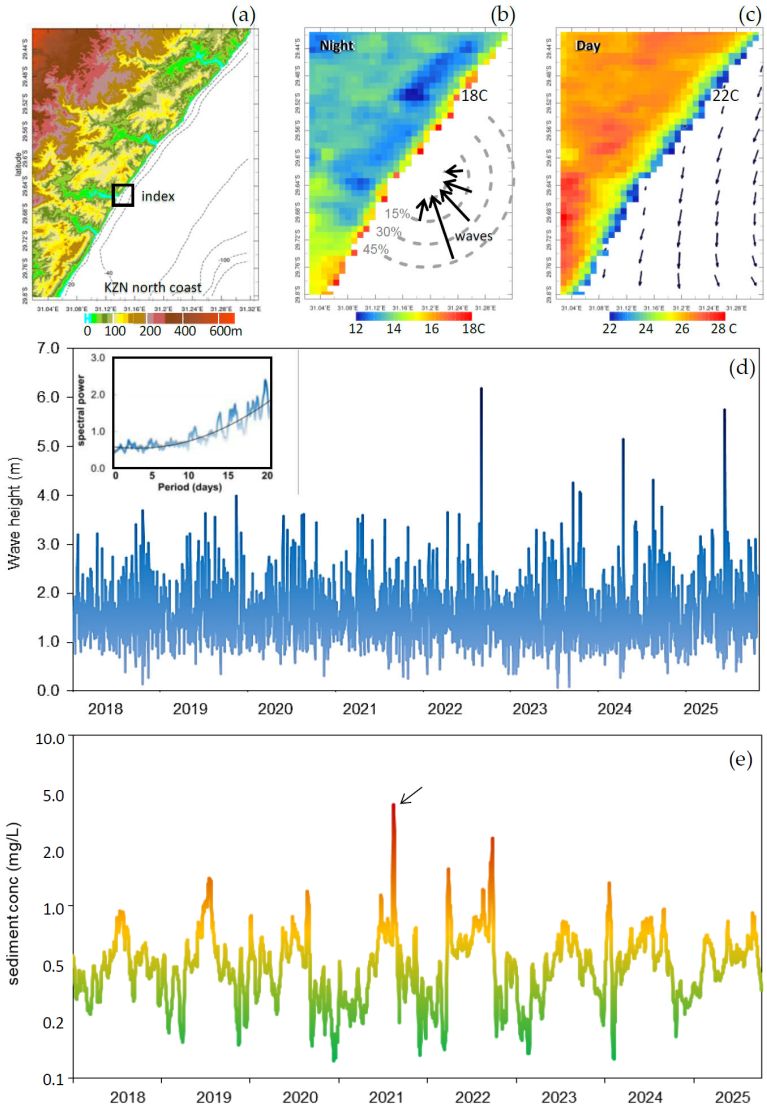


Figure 1. (**a**) Topography (shaded) and bathymetry (contours) of local study area with index (box). Satellite land surface temperatures averaged May–October (winter): (**b**) night-time map with wave direction frequency, (**c**) day-time map with mean currents (color bar varies). Index record of (**d**) daily wave height and (**e**) satellite sediment concentration (log-scale). Inset in (**b**) is wave direction frequency, inset in (**d**) is spectral power, and arrow in (**e**) points to case study.

Small estuaries, such as Tongaat (29.55 S, 31.15 E), are surrounded by sugar farming, commercial zones, and residential areas. Major highways cross the estuary, and the adjacent beach is exposed to frequent wind- and wave-action that accumulates drift-sand into tall

berms. The 425 km^2 catchment overflows ~80% of the time, dispersing sediments into the sea at concentrations > 1 mg/L that are re-worked by ~2 m tides and southeasterly swells [18]. During the dry winter season, the streamflow is weak, and sand dunes inhibit exchange. The average runoff ~74 Mm^3/yr passes through forests that host a biodiverse ecosystem with recreational appeal, yet about half the catchment landscape is degraded by informal settlements, unregulated sand mining, and agricultural and wastewater effluents that induce algal blooms and low-oxygen stress on the fishery [18]. Although high erosion rates can accumulate silt in the estuary and inhibit circulation, perennial discharges to the surf-zone expose sediments to wave-action and littoral drift, creating a dynamic environment [19]. The ecosystem is adapted to episodic flushing accompanied by turbulent winds and waves, yet a more static condition is desired to preserve ecotourism infrastructure [20]. This conundrum is regulated by zoning setbacks and access control, which leave room for tidal action. But a twin challenge has arisen from global warming: greater runoff and rising sea levels [21]. The scientific question to be answered is whether or not these counteractive processes can sustain the coastlines of northern KZN and beyond.

To provide scientific inferences, the nearshore suspended sediment concentration is estimated from satellite red-band reflectivity and statistically analyzed for environmental fluctuations at daily to seasonal time scales. The hypothesis is that streamflow runoff and wind–wave-induced sediments accumulate on northern KZN beaches at a rate similar to the erosion from rising seas, storm surges and land-use. Without field surveys, the sediment budget cannot be verified or 'closed'. Therefore, remote data are assessed to generate realistic estimates of surf-zone/aeolian transport and accretion rate/inundation risk to guide management decisions toward coastal resilience. This work is novel in that daily 2 km resolution products are employed to resolve the weather pulsing of the surf-zone 'conveyor'.

2. Data and Methods

High-resolution maps of bias-corrected long-term average NOAA multi-satellite land color and infrared temperature and level-3 EC multi-satellite ocean color reflectivity at ~0.6 μm, a proxy for turbidity and sediment concentration [22,23], were analyzed to provide spatial context over northern KZN: 29.42–29.80° S, 31.02–31.31° E. Weak longshore gradients implied that similar environmental conditions occur up and down the coast, thus a small area is representative of near-shore values. A 2 × 2 km coastal index area (centered on 29.65° S, 31.13° E, Mdloti river mouth) was identified for the extraction of daily environmental conditions over the period of 2018–2025, when measurements of 2 km resolution satellite ocean color are available.

Weather data were drawn from ERA5 [24] and MERRA2 reanalysis [25] and physical oceanography data from HYCOM3 [26] and GEFS wave reanalysis [27]. Table 1 lists the dataset characteristics. The time series (N = 2860) was analyzed for auto-correlation (persistence), wherein values become insignificant for wind at +2 days, and for rain and waves at +4 days, indicative of highly changeable marine weather in the southern sub-tropics.

Pair-wise cross-correlations were calculated between sediment concentration, meridional (V) surface wind and current, GEFS wave height, HYCOM3 surface salinity, rainfall and MERRA2 estimated runoff. Derived parameters include wind power and wave energy [28], whose formulation is described in Section 3.3. Statistical confidence is achieved with R > |0.25| from > 100 degrees of freedom.

Table 1. Datasets employed in the analysis.

Acronym	Name and Variables	Resolution
DE/GE	Digital Earth Africa, Google Earth CSIRO beach delineation, elevation profile	2 m annual
EC	European Community (Copernicus) Multi-satellite altimetry sea level	25 km day, month
EC	European Community (Copernicus) Multi-satellite ocean color (0.6 μm reflectivity)	0.3–2 km day, month
ERA5	European meteorology reanalysis v5 Coastal wind, rain, and air pressure	25 km hour, day
GEFS wave	Global Ensemble Forecast System Wave height, period, and direction assimilation	25 km hour, day
HYCOM3	Hybrid ocean model v3 Near-shore current, salinity assimilation	10 km day
IEM	Environmental Monitoring Wind rose at Durban airport	Point hour
MERRA2	American meteorology reanalysis v2 Atmospheric circulation, humidity, and runoff	50 km day, month
NASA/NOAA	National Space, Ocean & Atmosphere Admin Multi-satellite land color, land temperature, and OLR	25 km day, month
SA HYDRO	South African Hydrology Dept. Gauged streamflow (Msunduzi, Mvoti, and Tongaat)	Point day

The time series was analyzed for mean annual cycle and frequency distributions over the period of 2018–2025, and in situ-observed wind and wave roses were plotted. Sediment concentration crested > 1 mg/L in late winter (May–October), our seasonal focus in this study. This threshold identified daily values of vigorous surf-zone transport, whereas temporal statistics were constrained above 0.5 mg/L to capture a larger sample size. Lag-correlations were calculated to determine short-term response delays between daily coastal wind, rain, runoff, waves, and turbidity. Scatterplots were created to gain a better understanding of the functional relationships between coastal wind and current and between rain and runoff. Maps of high-resolution satellite ocean color reflectivity were analyzed for late-winter cases of high turbidity and associated surface salinity and currents.

Regional weather influences were quantified by regressing the daily record of index area sediment concentration onto fields of 500 hPa geopotential height, OLR (a proxy for cloud depth), and surface air pressure: 10–50° S, 5° W–65° E. A case of high sediment concentration during 5–7 September 2021 was studied via maps of satellite ocean color and currents, satellite OLR and surface winds, and a height section of atmospheric circulation on 31° E. The time series of local streamflow, ocean color, wave energy, and wind power was plotted to identify factors leading to sediment mobilization during 1–14 September 2021. These findings are underpinned by 20+ satellites that yield detailed information on nearshore color and altimetry [29].

Climatic influences were studied using multi-decade datasets filtered to retain cycles >18 months. These include monthly land color (vegetation) and runoff since 1981 [30] and ocean color reflectivity at ~0.6 μm since 1997, extensively validated for the estimation of the suspended sediment concentration in nearshore waters [31–34]. As in the statistical methods applied to the daily records mentioned above, lag correlations were calculated to determine seasonal response delays between coastal runoff, vegetation, and turbidity departures. Standardized runoff and vegetation records were averaged and regressed onto fields of SST and upper-level winds over the period of 1981–2025 to understand large-scale climatic features favoring locally high turbidity [16].

Multi-satellite sea surface height data were obtained [29] and trends were analyzed for sea level rise. To evaluate the impact of coastal sedimentation in northern KZN, 2 m resolution visible imagery and elevation profiles were obtained from Digital Earth Africa and Google Earth, and annual changes in the beach edge and profile at Westbrook (29.60° S, 31.15° E) were analyzed in the context of inundation risk [34,35].

The methodology followed a cascade of air–land–sea interactions: (i) sediment discharge in summer runoff, (ii) near-shore mixing and transport by winter wave-action [36], and (iii) fluctuating surf-zone and aeolian deposition on northern KZN beaches. The empirical statistics utilize daily 0.3–2.0 km resolution ocean color based on level-3 multi-satellite assimilation, a distinct advantage over earlier work that employed 4–9 km resolution weekly records with missing segments due to cloud-cover. Numerous validations justify the use of satellite ~0.6 μm red-band reflectivity to quantify near-shore turbidity from streamflow and wave-action [22,23,37–41].

3. Results

3.1. Coastal Features and Climate

A map of the northern KZN study area (Figure 1a) reveals a straight 210–030° coastline with steep hilly plains incised by a handful of small rivers. The tropical Agulhas Current flows southward 30 km seaward [42]. Winter-time land temperatures vary night-to-day (Figure 1b,c) from 13–27 °C over the interior to 18–22 °C on the coast. The alternating thermal gradient underpins land–sea breezes and diurnal–inertial currents. Waves from the southeast drive northward littoral drift over a seabed slope of ~2.6×10^{-2}.

The daily record of wave height (Figure 1d) exhibits chaotic pulsing from passing storms throughout the period of 2018–2025, averaging 1.5 m with a standard deviation of 0.6 m. Spectral power is significant at 3, 5, 11, and 15–20 days; there is a slight lull of wave-energy during summer. The daily record of satellite ocean color (estimated sediment concentration) exhibits lower values in summer and spikes of higher values in late winter (Figure 1e). This record forms the basis for empirical statistics.

Considering wind as a driver of air–land–sea interactions, Figure 2a presents the May–October wind rose from the nearby airport. Airflow is channeled in coastal alignment 210–030° with speeds frequently >5 m/s. Lag auto-correlation of daily V wind (Figure 2b) reveals a lack of persistence, $R < 0$ at +2 days. Near-shore HYCOM3 V currents at 10 m in the index area respond quickly to ERA5 marine winds; the scatterplot (Figure 2c) achieves $R^2 = 0.66$. The second-order regression exhibits a propensity for +V currents signifying northward littoral drift.

Winter V winds (Figure 2d) demonstrate a prominent lag correlation with index-area wave height at +1 day (R~0.49), and with rainfall at 0 and +1 day (R~0.27), but there is little persistence, indicating that hydrologic and oceanographic processes are pulsed by transient weather. Table 2 lists the simultaneous pair-wise correlation of daily records 2018–2025. Most Pearson R values are insignificant with respect to sediment concentration except for salinity (R = 0.37). We inferred opposition between the seasonal cycle and weather pulsing: winter's deep, mixed layer and big waves correspond with lower runoff. The simultaneous correlation of rainfall and runoff (R = 0.86) foretells steep slopes and small catchments with rapid flushing during wet spells. Another significant correlation is meridional winds and currents (R = 0.80). Together these reveal fast response times for air–land–sea interactions.

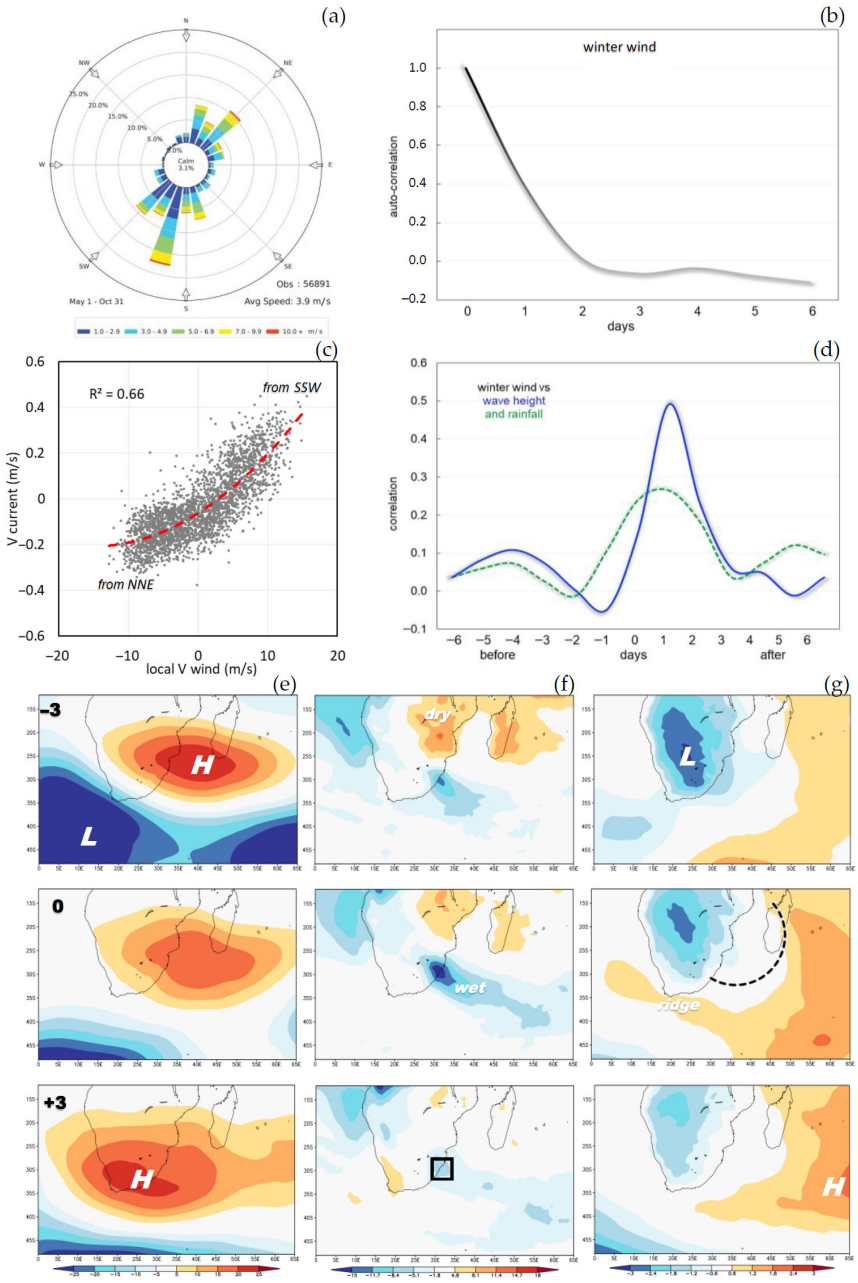


Figure 2. (**a**) May–Oct wind rose at DUR airport from hourly observations since 2018. (**b**) Lag auto-correlation of daily winter wind N = 1430. (**c**) Scatterplot of V wind vs. near-shore V current, 2018–2025. (**d**) Lag-correlation of May–October (winter) V wind with wave height and rainfall. Field regression of (**e**) 500 hPa height, (**f**) OLR field, and (**g**) surface air pressure onto daily satellite sediment concentration > 0.5 mg/L (cf. Figure 1e) at −3, 0, +3 days (top–down), with key features labeled.

Table 2. Simultaneous pair-wise cross-correlations of index area daily time series. Bold indicates significant, according to the effective degrees of freedom.

2018–2025	V Wind	Rainfall	V current	Salinity	Wave ht	Sediment
Rainfall	0.240					
V current	**0.798**	0.170				
Salinity	−0.011	−0.143	0.016			
Wave ht	0.054	0.096	0.082	−0.011		
Sediment	−0.001	−0.090	0.047	**0.367**	0.014	
Runoff	0.182	**0.864**	0.130	−0.107	0.074	−0.053

3.2. Climatic Influences on Sediment Concentration

Regressing the daily sediment concentration (>0.5 mg/L) onto fields of 500 hPa geopotential height, OLR, and surface air pressure from −3 to +3 days (Figure 2e–g), certain weather patterns emerge. An upper high and surface low in the sub-tropics and a mid-latitude low feature prominently. A NW cloud-band, indicated by –OLR, focuses rainfall over northern KZN, while sunny conditions (+OLR) occur in the tropics further north. On day 0, a surface ridge extends across the mid-latitudes, leading to on-shore airflow and waves during spells of high sediment concentration.

Figure 3a presents a high-resolution satellite ocean color image from 22 October 2025: surf-zone sediments decline rapidly seaward, and along-shore gradients are weak. A few days before the image, a storm had passed with 3.5 m waves from 190° at 14 s interval, accompanied by SSE winds ~14 m/s and rainfall ~20 mm. Hence, the coastal zone received pulses of runoff that joined turbulent re-worked sediment in northward littoral drift. The long-term average vegetation fraction ~0.35 (Figure 3a) is indicative of landscapes transformed for sugar farming and residential development, which generate sediment discharge during fast runoff. Dense forests with vegetation fraction >0.5 can retain sediments, but only cover ~5% of the coastal plains in northern KZN.

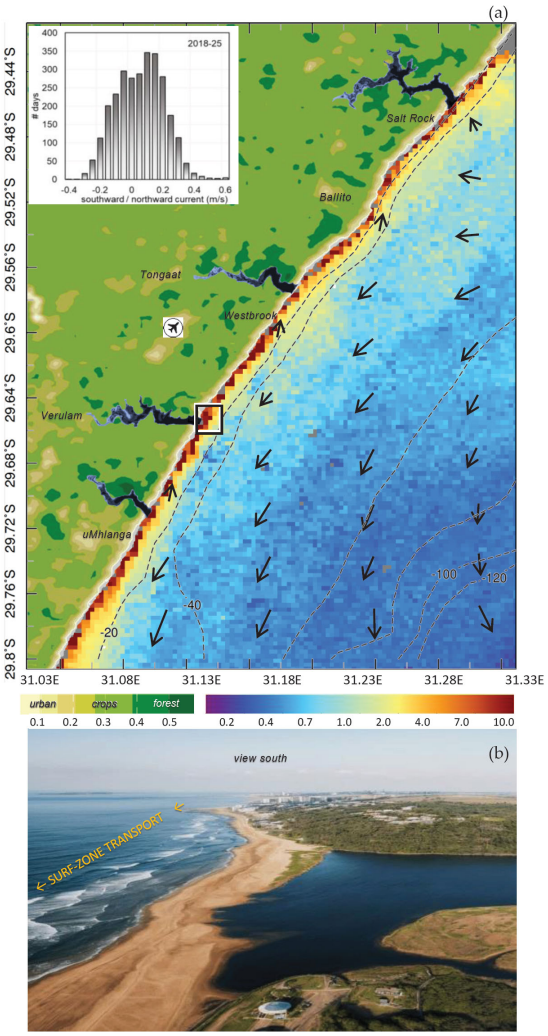


Figure 3. (**a**) 300 m resolution satellite sediment concentration (log-scale, mg/L) and HYCOM3 surface layer currents (vector, largest 0.2 m/s) on 22 October 2025; inset is current histogram N = 2860. Index box, place names, DUR airport, average vegetation fraction, and river mouths overlain. (**b**) Aerial view of the index area, looking south across the Mdloti river mouth.

Of particular interest are the near-shore currents on 22 October 2025, indicative of a surf-zone conveyor. The inset (Figure 3a) is a frequency histogram of V currents, exhibiting a major peak +0.2 m/s (northward) and a minor peak −0.1 m/s (southward). Thus, re-working occurs in both directions, but northward drift prevails.

Figure 3b provides an aerial photo of the index area, Mdloti river mouth and beach-front. Catchment vegetation is dense, and ecotourism development is evident in the distance (uMhlanga). As noted earlier, these rivers overflow ~80% of the time, and the mouths are characterized by tall berms that recycle sand to the surf-zone under 2 m tides and storm surge [18].

Rainfall in northern KZN naturally contributes to runoff (Figure 4a inset). The daily scatterplot regression with $R^2 = 0.75$ has a conversion rate of 11.6%. Salinity is therefore low near the coast (Figure 4a) and its temporal record (Figure 4b) dips and crests following the seasonal climate (35.2–35.4 ppt, cf. [43]). The influx of freshwater and surface heating induce buoyancy in late summer (Figure 4c). The stratification inhibits turbulent mixing to a depth of < 20 m. Wave-action from Nov–Apr seldom lifts sand off the seabed.

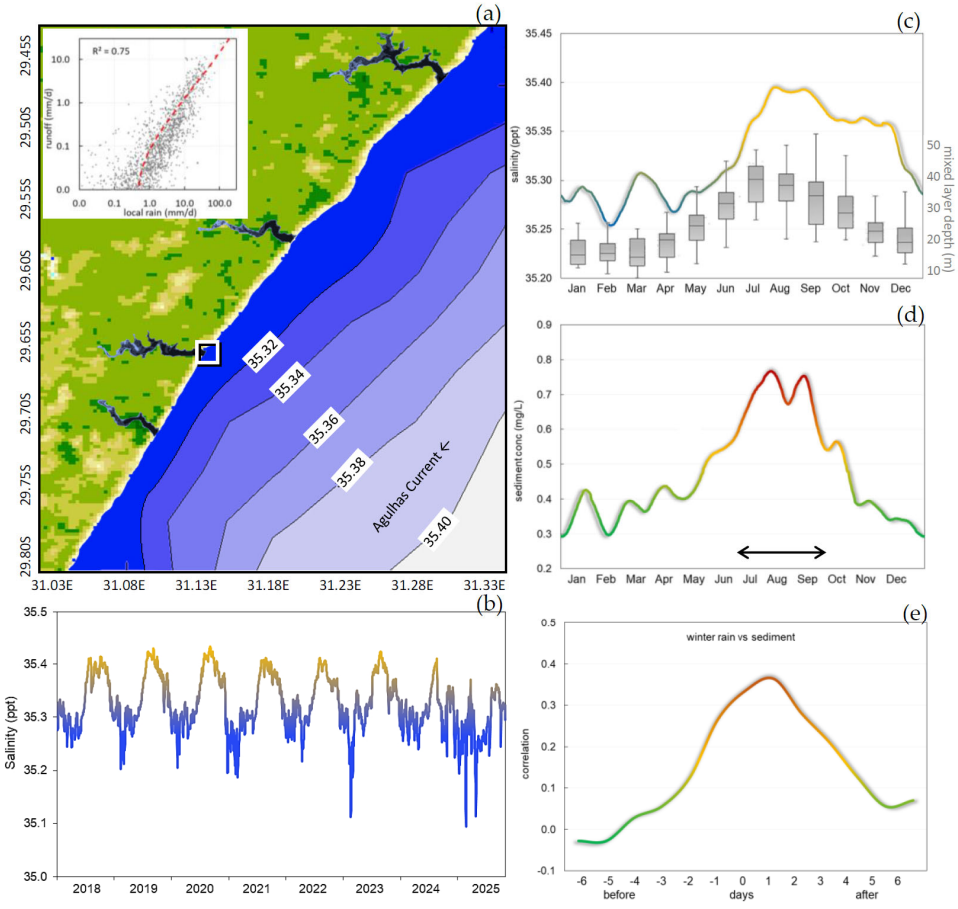


Figure 4. (**a**) HYCOM3 salinity on 22 October 2025 with river mouths, vegetation, and index box; inset is log-rain vs. runoff scatterplot. (**b**) Daily record of salinity, 2018–2025. Mean annual cycle of (**c**) HYCOM3 salinity, mixed-layer depth and (**d**) satellite sediment concentration. (**e**) Lag correlation of May–October (winter) rainfall vs. sediment concentration > 0.5 mg/L.

The mean annual cycle of surf-zone sediment concentration (Figure 4d) reveals a late-winter peak in Jun–Oct that coincides with deep oceanic mixing ~40 m. Pulses of high turbidity follow wet spells, as revealed by lag correlation with daily rainfall in Figure 4e ($R \sim 0.38$ at +1 day, $N = 1430$). Hence, northern KZN beaches are most dynamic in late winter, as wave-action entrains sediments into the surf-zone conveyor. Subsequent dry

windy spells encourage aeolian deposition, where coastal infrastructure and vegetation leave sufficient space.

3.3. Sediment Dispersion and Case Study

Stepping back from empirical statistics, the two key processes of sediment dispersion, surf-zone wave-action and wind-borne accumulation, are formulated. Average waves of 1.5 m from ±160° at 7 s intervals generate wave energy [28,44,45]: $E = \int (H^2\ T \sin \theta) = 7$ kW/m (H—height, T—period, and θ—refraction angle). During late winter, the average waves increase to 1.8 m at 8 s intervals, so E nearly doubles to 13 kW/m and is more effective in mobilizing seabed sediments under surface cooling and a deep, mixed layer.

Sediment transport is a product of surf-zone current (Vc) and suspended sediment concentration [36,45,46]. In situ measurements indicate northward drift ~0.3 m/s, consistent with theory: $Vc = 7(S)(gH \sin \theta)^{0.5}$ [28] (S—seabed slope, 2.6×10^{-2}, with H and θ as above). With long-term average sediment concentration ~0.5 mg/L, the long-shore transport in the surf-zone is ~1.5×10^4 kg/yr/m. Under late-winter wave-action, potential deposition can exceed 10^5 kg/yr/m. Re-working tends to disperse sediments according to grain size: coarser sands move on-shore while finer silts remain off-shore [47].

Aeolian transport is a function of wind power $W = (\rho/2)V^3$ [28]. For an air density of 1.2 kg/m^3 and daily wind gusts on the beaches of northern KZN, the average power is 72 W/m^2. Wind power reaches 500 W/m^2 during cyclonic storms, but airborne sand mobilization is damped by rainy weather [4]. In dry windy spells, beach sands with grain sizes 240–410 µm achieve aeolian transport > 10^3 kg/yr/m. Deposition is aided by the convergence of NE winds (-10^{-2} s^{-1}) and by shoreward refraction of SE waves [17]. The beachfront berms accumulate sand and re-vegetate, growing and shedding seaward [20].

Although summer rainfall stimulates runoff and streamflow, it is during late winter that deep mixing enables high wave energy to scour the seabed and disperse sediments northward. In application, consider the case of September 2021. Satellite sediment concentration (Figure 5a) exceeded 1 mg/L in the surf-zone on 7 September 2021. Turbulent currents (Figure 5b) swept the seabed, lifting sand for northward transport (Figure 5c). A ridging high/cut-off low weather pattern on 6 Sep induced atmospheric convection along the coast (Figures 5d and A1). The meridional airflow formed a moist rotor over northern KZN (30° S) beneath an anomalous jet stream (Figure 5e) with dry zones on either side (40° S, 20° S). Cool, moist on-shore winds passed across the tropical Agulhas Current.

Index-area temporal records during 1–14 September 2021 (Figure 5f,g) indicate a streamflow of 7 m^3/s coincided with high turbidity. Wave energy spiked > 50 kW/m before and during the event, and wind power reached 600 W/m^2 on 7 September, as the ridging high/cut-off low pattern drove marine airflow onto the steep coastal plains of northern KZN cf. [48]. A combination of runoff and wind- and wave-action contributed to this late-winter case of coastal sediment dispersion.

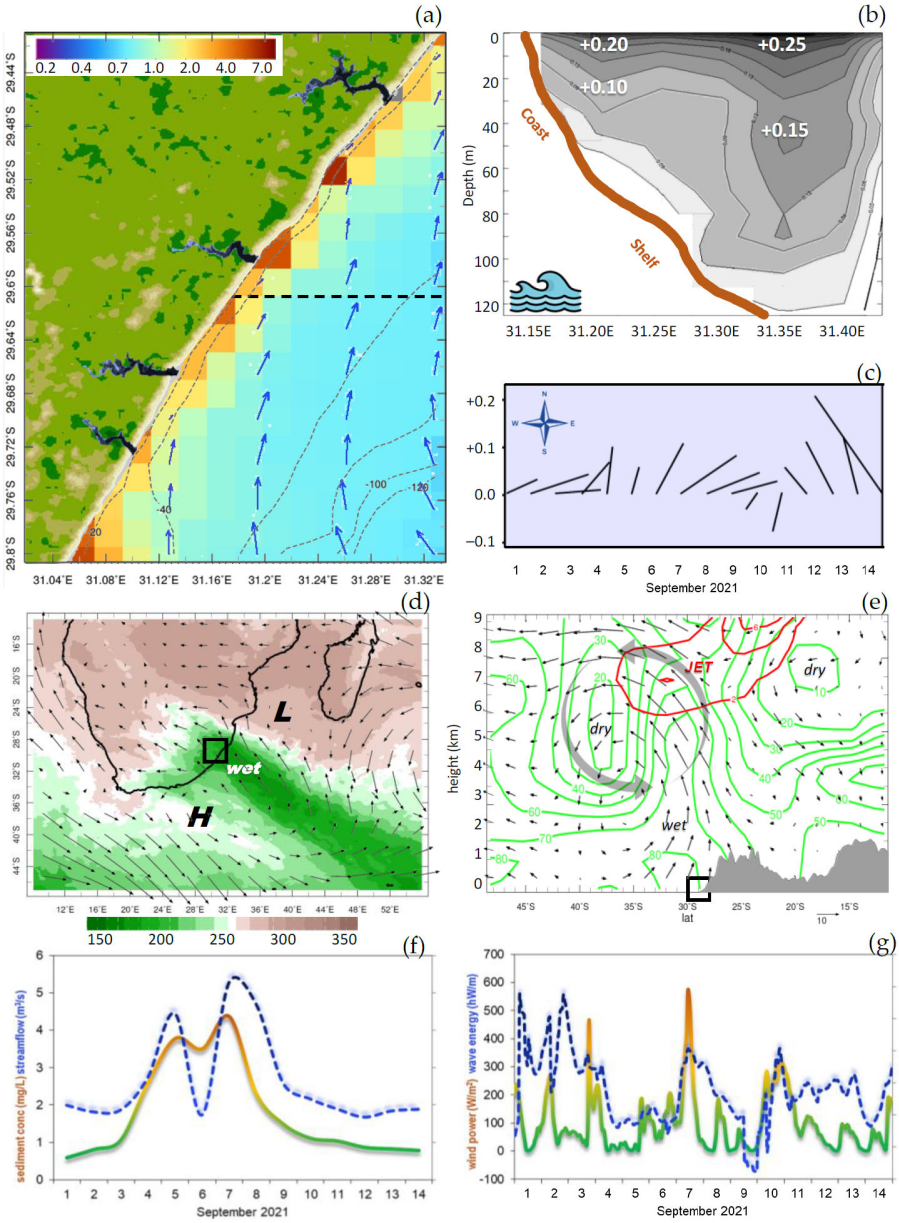


Figure 5. Case study of September 2021: (**a**) 2 km resolution satellite sediment concentration (mg/L) on 7 September, with vegetation, river mouths, and surface currents (vector, largest 0.3 m/s), (**b**) depth section on 29.6 S (dashed in (**a**)) of HYCOM3 northward currents, and (**c**) daily record of near-shore currents (sticks, m/s). Weather conditions for 6 September 2021: (**d**) Map of surface winds (vector) and OLR (shaded), (**e**) height section on 31 E of meridional circulation (vector), humidity (green contour), +U wind anomalies (red contour), key area (box). Time series of northern KZN for 1–14 September 2021: (**f**) measured streamflow (dashed) and satellite sediment concentration, and (**g**) GEFS wave energy (dashed) and ERA5 wind power.

3.4. Long-Term Climate Influence

It is helpful to place the transient environmental conditions in a broader context of long-term trends and associated processes. Runoff is greater in southern KZN due to the steep slope next to the 3000 m high Drakensberg Mountains (Figure 6a). Prevailing SSE waves drive a surf-zone conveyor, which entrains sediments northward past Durban.

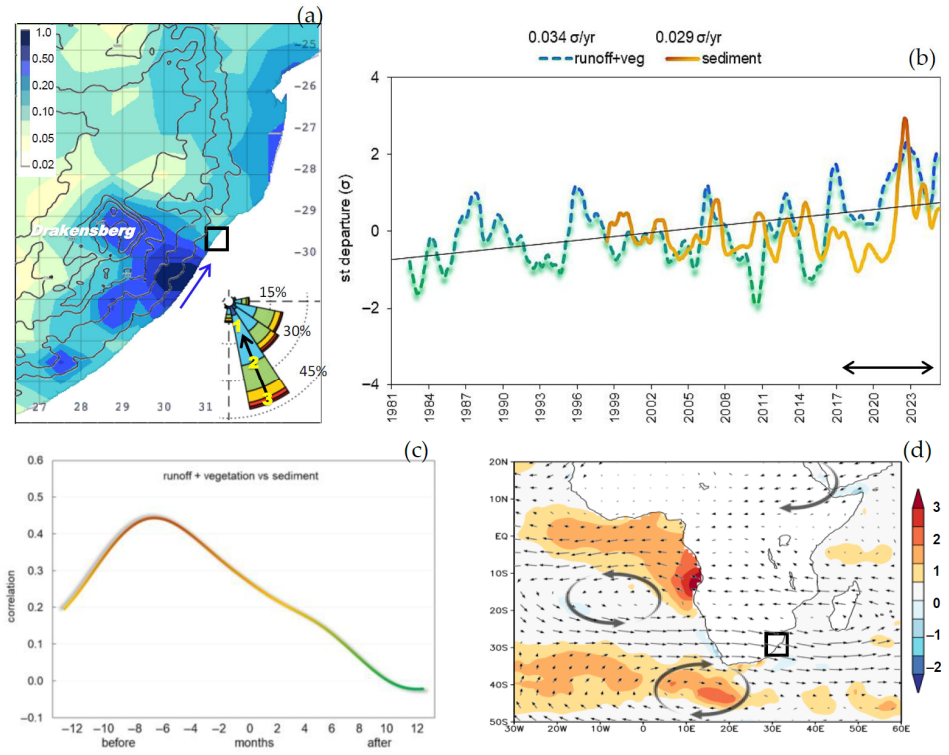


Figure 6. (**a**) Map of average runoff, inset wave rose (after [8]), and surf-zone current (arrow). (**b**) Index-area filtered standardized time series and trend with daily era delineated. (**c**) Lag correlation of filtered runoff + vegetation vs. sediment concentration, noting summer to winter delay. (**d**) Time–space regression of filtered runoff + vegetation departures during the period of 1982–2024 onto the regional field of SST and upper wind (vector): Atlantic warming and circulation anomalies.

Temporal records of index-area filtered monthly runoff, land color (vegetation), and ocean color (sediment) exhibit significant upward trends: 0.029–0.034 σ/yr since 1981 (Figure 6b). Lag correlations (Figure 6c) show that runoff and vegetation were leading causes of sedimentation (R ~ 0.44 at −7 months), indicating that a wet summer is followed by a stormy winter.

The climatic influence is mapped by point-to-field regression of runoff + vegetation vs. SST and upper wind in Figure 6d. Oceanic warming in the SE Atlantic accelerates the subtropical jet stream, contributing to late-winter storms that stimulate sedimentation. The cut-off low/ridging high weather pattern has become more frequent due to global warming and the meandering of upper westerly winds [49,50]. The runoff + vegetation record exhibits rhythmic 8-year oscillations since 1981, followed by 5-year oscillations since 1998, providing a mechanism for beach advance and retreat, superimposed on upward trends which account for 23% of variance (R^2).

Figure 7a illustrates how quickly sediment concentration declines away from the coast. Long-term average surf-zone values exceed 1 mg/L during late winter storms, delivering sand that could accumulate, if not for the counteracting effect of rising sea level ~0.6 cm/yr (Figure 7b).

The risk of inundation is evaluated from extreme value statistics for wave height and air pressure: $0.15H + (1012 - P) \times 0.1$. Although big waves seldom coincide with low pressure in northern KZN, extreme values of H = 6 m and P = 995 hPa have been recorded during the passage of mid-latitude lows. Adding L = 2.4 m local spring tide and S = 0.5 m global sea-level rise by mid-century, the potential inundation is H + P + L + S = 5.5 m under storm surge. Applied to the Westbrook elevation profile (Figure 7c,d), over-wash reaches ~25 m inland, affecting coastal infrastructure in a globally warmed future [2,35]. Yet the beach edge has advanced ~10 m between 2017 and 2024, likely due to an upturn of sediment

dispersion within long-term trends [8,51]. Despite rising sea level and recreational use, aeolian berms have accumulated at a rate of ~1 T/m over the past few decades (dashed in Figure 7d), suggesting physical resilience that deserves careful management.

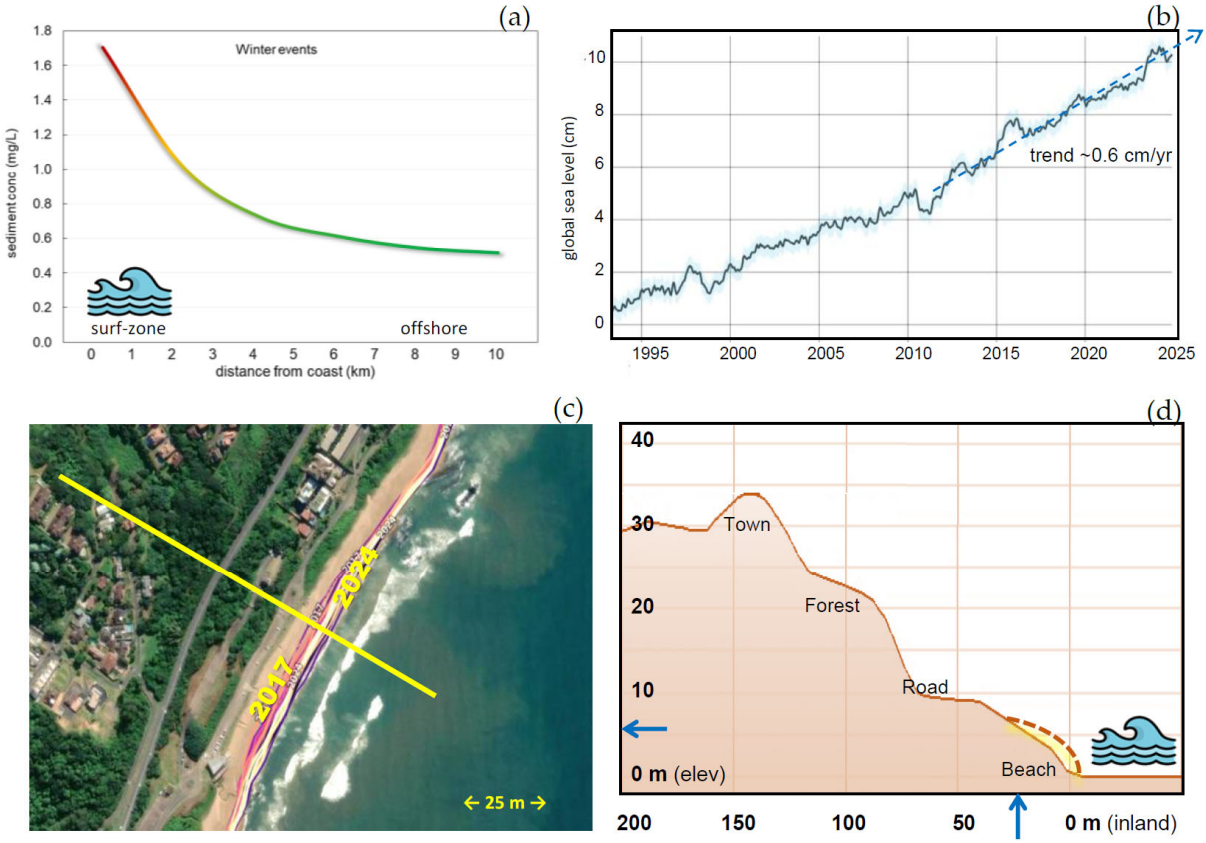


Figure 7. (**a**) Average cross-shore sediment concentration on winter days with higher values. (**b**) Global sea level time series from satellite altimetry. (**c**) Satellite image of Westbrook beach with annual edge delineated (from Digital Earth Africa), and (**d**) elevation profile along the yellow line (from Google Earth), with a 5.5 m inundation level (blue arrows); dashed area suggests accretion rate during the period of 2017–2024.

4. Concluding Discussion

This study of air–land–sea interactions on the shores of northern KwaZulu-Natal has focused on the highly variable nature of local runoff, wave-action and turbidity. This work is novel in using daily high-resolution multi-satellite assimilation, while earlier work had to contend with coarse temporal and spatial products that could not resolve the pulsing of the surf-zone conveyor. Although a sea-level rise of 0.6 cm/yr brings risks of coastal erosion and shoreline retreat, the sediment flux from streamflow and surf-zone dispersion provides a counteracting mechanism capable of sustaining or even advancing sections of the coastline.

Daily observations during the period of 2018–2025 (cf. Table 2, Figure 4b) reveal transient sediment dispersion, suggesting the opposition of the annual cycle and weather pulsing. The small catchments of northern KZN discharge seaward within one day of rainy weather. Similarly, winter wind and wave turbulence exhibit little persistence, pulsing sediments in the surf-zone conveyor at 3–5 day intervals (cf. Figures 1d and 4e). Although most runoff occurs in summer, sediment concentrations peak during late winter when deep mixing and elevated wave energy (>13 kW/m) mobilize deposits previously sequestered under buoyant, stratified conditions, similar to [39]. The case of September 2021 illustrated how a ridging high/cut-off low weather pattern induced on-shore airflow and shallow

convection that simultaneously increased streamflow, wave energy, wind power, and sediment dispersion.

Long-term climate diagnostics found that hydrological variability is governed by the warming of the southeast Atlantic and intensified sub-tropical upper-level westerlies. Late-winter storms are generated that mobilize sediments in a 5–8 year cycle (Figure A2), leading to shoreline advance and retreat [8,9]. The association between upstream weather patterns and downstream impacts relies on statistical inferences. Over the past four decades, upward trends in coastal runoff, vegetation, and sediment concentration (0.29 σ/yr) suggest an amplified water cycle contributing to beach stability at Westbrook KZN, despite rising seas and urbanization. The Digital Earth Africa [52] map (Figure 7c) exhibited local coastline advance during the period of 2017–2024 due to an accretion of ~ 1 T/m despite storm surge inundations of ~5.5 m; longer-term records are needed to verify equilibrium. Looking up and down the coast of Africa with Digital Earth, it is noted that about one-quarter of all beaches are accreting while about one-third are eroding, particularly in major river deltas with upstream offtake.

Although remote information could not close the sediment budget, realistic estimates of long-shore transport in the surf-zone (~1.5×10^4 kg/yr/m) and on the beach (>10^3 kg/yr/m) were presented. The water-borne component is an order of magnitude greater than airborne due to convex coastal exposure to mid-latitude wave action, and narrow sand margin backed by urbanized or vegetated slopes. These findings imply that northern KZN's beaches are not passively regressive systems but dynamic landforms whose resilience depends on maintaining natural air–land–sea feedbacks. Where catchments continue to generate runoff and where the littoral system remains unobstructed, late-winter storms can sustain dune growth. Conversely, sediment diversion for water use and beachfront hardening would limit the natural buffering capacity and increase exposure to inundation up to 25 m inland (cf. Figure 7d).

In summary, the northern KZN coastline exhibits conditional resilience: global sea-level rise increases hazard potential, but enhanced sediment fluxes—tied to a faster water cycle and winter storms—presently offset these pressures. This balance is delicate, but evidence suggests equilibrium for many coastlines [12,52]. Effective management should therefore prioritize: (i) maintaining sediment connectivity from catchment to coast, (ii) preserving space for dune mobility, (iii) monitoring estuarine water quality and river-mouth dynamics, and (iv) anticipating the climatic modulation of sediment supply. Sustaining these processes will support coastal ecotourism infrastructure in a warming world.

Funding: This research received no external funding.

Data Availability Statement: The raw data supporting the conclusions of this article will be made available by the authors on request.

Acknowledgments: Data were analyzed from NASA-giovanni, IRI-climate library, Climate Explorer-knmi, University Hawaii-adprc, Digital Earth Africa, Google Earth, and SA Hydrology websites. Indirect support from the South Africa Department of Higher Education is noted.

Conflicts of Interest: The authors declare no conflict of interest.

Appendix A

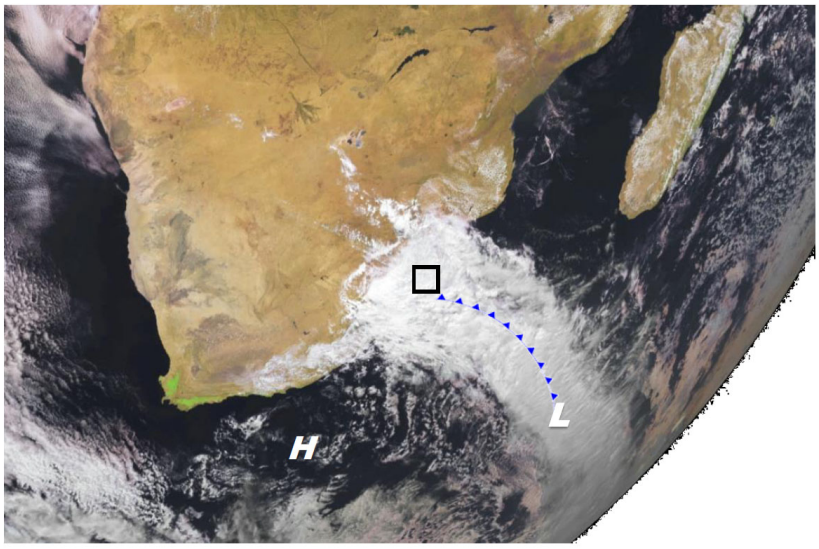


Figure A1. Meteosat image from 7 September 2021, indicating the case study weather and index area, blue icon is a cold front.

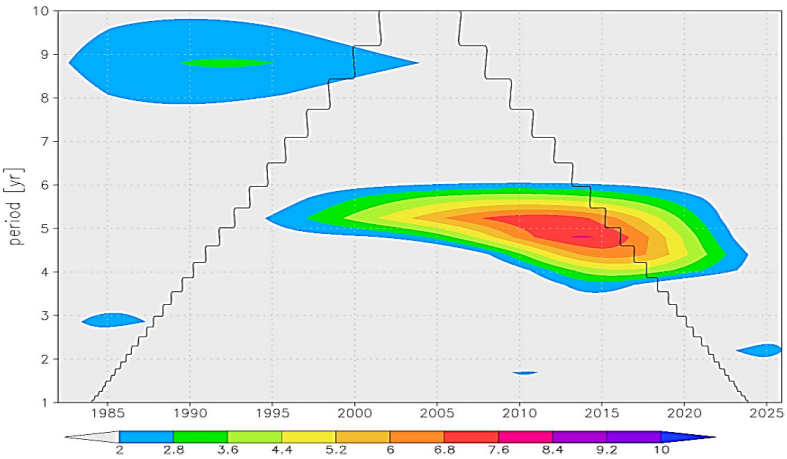


Figure A2. Wavelet spectral analysis of the filtered runoff + vegetation record, cf. Figure 6b; shaded > 90% confidence reveals 5 and 8 yr cycling of northern KZN hydrology, within the cone of validity.

References

1. Nicholls, R.J.; Cazenave, A. Sea-Level Rise and Its Impact on Coastal Zones. *Science* **2010**, *328*, 1517–1520. [CrossRef] [PubMed]
2. Vitousek, S.; Barnard, P.; Fletcher, C.; Frazer, N.; Erikson, L.; Storlazzi, C. Doubling of coastal flood exposure in the 21st century due to sea-level rise. *Sci. Adv.* **2017**, *3*, e1700573.
3. IPCC. *Climate Change 2021: The Physical Science Basis*; Cambridge University Press: Cambridge, UK, 2023; 2338p.
4. Pethick, J.; Carter, R.W.G. *Coastal Environments: An Introduction to the Physical, Ecological and Cultural Systems of Coastlines*; Academic Press: London, UK, 1988; p. 617.
5. Van Rijn, L.C. *Principles of Sediment Transport in Rivers, Estuaries and Coastal Seas*; Aqua Publications: Blokzijl, The Netherlands, 1993; p. 20.
6. Syvitski, J.P.M.; Vörösmarty, C.J.; Kettner, A.J.; Green, P. Impact of Humans on the Flux of Terrestrial Sediment to the Global Coastal Ocean. *Science* **2005**, *308*, 376–380. [CrossRef] [PubMed]
7. O'Grady, J.; Babanin, A.; McInnes, K. Downscaling Future Longshore Sediment Transport in South Eastern Australia. *J. Mar. Sci. Eng.* **2019**, *7*, 289. [CrossRef]
8. Corbella, S.; Stretch, D.D. Decadal trends in beach morphology on the east coast of South Africa and likely causative factors. *Nat. Hazards Earth Syst. Sci.* **2012**, *12*, 2515–2527. [CrossRef]
9. Smith, A.; Guastella, L.; Botes, Z.; Bundy, S.; Mather, A. Forecasting cyclic coastal erosion on a multi-annual to multi-decadal scale: Southeast African coast. *Estu. Coast. Shelf Sci.* **2014**, *150*, 86–91. [CrossRef]

10. Warrick, J.A.; Stevens, A.W.; Miller, I.M.; Harrison, S.R.; Ritchie, A.C.; Gelfenbaum, G. World's largest dam removal reverses coastal erosion. *Sci. Rep.* **2019**, *9*, 1–12. [CrossRef]
11. Corbella, S.; Stretch, D.D. The wave climate on the KwaZulu-Natal coast of South Africa. *J. S. Afr. Inst. Civil Eng.* **2012**, *54*, 45–54.
12. Mentaschi, L.; Vousdoukas, M.I.; Pekel, J.-F.; Voukouvalas, E.; Feyen, L. Global long-term observations of coastal erosion and accretion. *Sci. Rep.* **2018**, *8*, 12876. [CrossRef]
13. Jury, M.R. Historical and projected climatic trends in KwaZulu-Natal: 1950–2100. *Water SA* **2022**, *48*, 369–379. [CrossRef]
14. Fowler, M.D.; Kooperman, G.J.; Randerson, J.T.; Pritchard, M.S. The effect of plant physiological responses to rising CO_2 on global streamflow. *Nat. Clim. Change* **2019**, *9*, 873–879. [CrossRef]
15. Xie, J.; Liu, X.; Jasechko, S.; Berghuijs, W.R.; Wang, K.; Liu, C.; Reichstein, M.; Jung, M.; Koirala, S. Majority of global river flow sustained by groundwater. *Nat. Geosci.* **2024**, *17*, 770–777. [CrossRef]
16. Jury, M.R. Modulation of the Marine Environment in the Natal Bight. *Remote Sens.* **2023**, *15*, 1434. [CrossRef]
17. Jury, M.R. Meteorological controls on big waves south of Africa. *Reg. Stud. Mar. Sci.* **2019**, *27*, 100538. [CrossRef]
18. Dawson, J.; Hutchings, K.; Sedick, S.; Clark, B.M. *uTongaat Estuary Management Plan Final Report*; Report no. 1905/9; Anchor Research & Monitoring (Pty) Ltd.: Cape Town, South Africa, 2021; p. 83.
19. Tinley, K.L. *Coastal Dunes of South Africa*; Foundation for Research Development: Pretoria, South Africa, 1985; p. 300.
20. Wang, H.; Liu, X.; Wang, K.; Liu, C. Response of Global Runoff Components to Rising CO_2. *Earth's Futur.* **2024**, *12*, e2024EF005091. [CrossRef]
21. Ouillon, S.; Douillet, P.; Petrenko, A.; Neveux, J.; Dupouy, C.; Froidefond, J.-M.; Andréfouët, S.; Muñoz-Caravaca, A. Optical Algorithms at Satellite Wavelengths for Total Suspended Matter in Tropical Coastal Waters. *Sensors* **2008**, *8*, 4165–4185. [CrossRef]
22. Lu, J.; Chen, X.; Tian, L.; Zhang, W. Numerical simulation-aided MODIS capture of sediment transport for the Bohai Sea in China. *Int. J. Remote Sens.* **2014**, *35*, 4225–4238. [CrossRef]
23. Hersbach, H.; Bell, B.; Berrisford, P.; Hirahara, S.; Horányi, A.; Muñoz-Sabater, J.; Nicolas, J.; Peubey, C.; Radu, R.; Schepers, D.; et al. The ERA5 global reanalysis. *Q. J. R. Meteorol. Soc.* **2020**, *146*, 1999–2049. [CrossRef]
24. Gelaro, R.; McCarty, W.; Suárez, M.J.; Todling, R.; Molod, A.; Takacs, L.; Randles, C.A.; Darmenov, A.; Bosilovich, M.G.; Reichle, R.; et al. The modern-era retrospective analysis for research and applications, version 2 (MERRA-2). *J. Clim.* **2017**, *30*, 5419–5454. [CrossRef]
25. Chassignet, E.P.; Hurlburt, H.E.; Metzger, E.J.; Smedstad, O.M.; Cummings, J.A.; Halliwell, G.R.; Bleck, R.; Baraille, R.; Wallcraft, A.J.; Lozano, C.; et al. US GODAE: Global Ocean Prediction with the HYbrid Coordinate Ocean Model (HYCOM). *Oceanography* **2009**, *22*, 64–75. [CrossRef]
26. Alves, J.-H.; Padilla-Hernandez, R.; Spindler, D.; Kolczynski, W.; Rajan, B.; Spindler, T.; Abdolali, A.; Campos, R.; Banihashemi, S.; Meixner, J. Development of a Wave Model Component in the First Coupled Global Ensemble Forecast System at NOAA. *Weather Forecast.* **2024**, *39*, 1761–1776. [CrossRef]
27. Van Rijn, L.C. Principles of sediment transport in coastal environments. *J. Hydraulic Eng.* **2009**, *135*, 196–203.
28. 28Copernicus Marine. Global Sea Surface Height Analysis. European Community Data Store. Available online: https://data.marine.copernicus.eu/product/OCEANCOLOUR_GLO_BGC_L3_MY_009_103/notifications (accessed on 1 December 2025).
29. Pinzon, J.E.; Tucker, C.J. A non-stationary 1981–2012 AVHRR NDVI3g time series. *Remote Sens.* **2014**, *6*, 6929–6960. [CrossRef]
30. Han, B.; Loisel, H.; Vantrepotte, V.; Mériaux, X.; Bryère, P.; Ouillon, S.; Dessailly, D.; Xing, Q.; Zhu, J. Development of a Semi-Analytical Algorithm for the Retrieval of Suspended Particulate Matter from Remote Sensing over Clear to Very Turbid Waters. *Remote Sens.* **2016**, *8*, 211. [CrossRef]
31. Balasubramanian, S.V.; Pahlevan, N.; Smith, B.; Binding, C.; Schalles, J.; Loisel, H.; Gurlin, D.; Greb, S.; Alikas, K.; Randla, M.; et al. Robust algorithm for estimating total suspended solids (TSS) in inland and nearshore coastal waters. *Remote Sens. Environ.* **2020**, *246*, 111768. [CrossRef]
32. Tshazi, Z. Estimating Estuarine Suspended Sediment Concentration Through Spectral Indices and Band Ratios Derived from Sentinel-2 Data: A Case of Umzimvubu Estuary, South Africa. Master's Thesis, University of Fort Hare, Dikeni, South Africa, 2022. Available online: https://files01.core.ac.uk/download/591353960.pdf (accessed on 1 December 2025).
33. Teng, W.; Qian, Y.; Dariusz, S.; Reynols, R.A.; Woodruff, J.D.; Yellen, B. High spatial-resolution satellite mapping of suspended particulate matter in global coastal waters using particle composition-adaptive algorithms. *Remote Sens. Environ.* **2025**, *323*, 114745. [CrossRef]
34. Figlus, J.; Kobayashi, N.; Gralher, C.; Iranzo, V. Wave Overtopping and Overwash of Dunes. *J. Waterw. Port, Coastal, Ocean Eng.* **2011**, *137*, 26–33. [CrossRef]
35. van Rijn, L.C. Unified View of Sediment Transport by Currents and Waves. II: Suspended Transport. *J. Hydraul. Eng.* **2007**, *133*, 668–689. [CrossRef]
36. Kaliraj, S.; Chandrasekar, N.; Magesh, N.S. Impacts of wave energy and littoral currents on shoreline erosion/accretion along the south-west coast of Tamil Nadu. *Environ. Earth Sci.* **2013**, *71*, 4523–4542. [CrossRef]

37. Dogliotti, A.; Ruddick, K.; Nechad, B.; Doxaran, D.; Knaeps, E. A single algorithm to retrieve turbidity from remotely-sensed data in all coastal and estuarine waters. *Remote Sens. Environ.* **2015**, *156*, 157–168. [CrossRef]
38. Valente, A.; da Silva, J.C.B.; Brotas, V. Sediment dynamics in surf zones under storm conditions. *Mar. Geol.* **2021**, *440*, 106533.
39. Wilson, G.W.; Dickhudt, P.; Aldrich, J. Sediment Dynamics in the Energetic Nearshore Zone: Acoustic Remote Sensing and Model Validation. *J. Geophys. Res. Oceans* **2024**, *129*, e2024JC021563. [CrossRef]
40. Kong, Y.; Jimenez, K.; Lee, C.M.; Winter, S.; Summers-Evans, J.; Cao, A.; Menczer, M.; Han, R.; Mills, C.; McCarthy, S.; et al. Monitoring Coastal Water Turbidity Using Sentinel2—A Case Study in Los Angeles. *Remote Sens.* **2025**, *17*, 201. [CrossRef]
41. Guastella, L.; Roberts, M. Dynamics and role of the Durban cyclonic eddy in the KwaZulu-Natal Bight ecosystem. *Afr. J. Mar. Sci.* **2016**, *38*, S23–S42. [CrossRef]
42. Jury, M.R. Modulation of currents near Durban. *Reg. Stud. Mar. Sci.* **2018**, *18*, 208–218. [CrossRef]
43. Miller, H.C. Field measurements of longshore sediment transport during storms. *Coast. Eng.* **1999**, *36*, 301–321. [CrossRef]
44. Van Wellen, E.; Chadwick, A.; Mason, T. A review and assessment of longshore sediment transport equations for coarse-grained beaches. *Coast. Eng.* **2000**, *40*, 243–275. [CrossRef]
45. Esteves, L.S.; Williams, J.J.; Lisniowski, M.A. Measuring and modelling longshore sediment transport. *Estuarine, Coast. Shelf Sci.* **2009**, *83*, 47–59. [CrossRef]
46. Sawczynski, S.; Kaczmarek, L. Sediment transport in the coastal zone. *Tech. Sci.* **2014**, *17*, 165–180.
47. Jury, M.R. Meteorology of 'ridging high' rainfall over the KwaZulu-Natal coastal plains. *Int. J. Clim.* **2023**, *43*, 7516–7531. [CrossRef]
48. Moon, W.; Kim, B.-M.; Yang, G.-H.; Wettlaufer, J.S. Wavier jet streams driven by zonally asymmetric surface thermal forcing. *Proc. Natl. Acad. Sci. USA* **2022**, *119*, e2200890119. [CrossRef]
49. Shaw, T.A.; Miyawaki, O.; Chou, H.-H.; Blackport, R. Fast-get-faster explains wavier upper-level jet stream under climate change. *Commun. Earth Environ.* **2024**, *5*, 1–10. [CrossRef]
50. Sorensen, R. Coastal Zone Processes. In *Basic Coastal Engineering*; Springer: Boston, MA, USA, 2006; pp. 247–286. [CrossRef]
51. Digital Earth Africa. CSIRO Annual Beach Delineation and Shoreline Changes 2001–2025. 2005. Available online: https://digitalearthafrica.org/en_za/coastlines/ (accessed on 1 December 2025).
52. Jury, M.R. Links Between the Coastal Climate, Landscape Hydrology, and Beach Dynamics near Cape Vidal, South Africa. *Coasts* **2025**, *5*, 25. [CrossRef]

Disclaimer/Publisher's Note: The statements, opinions and data contained in all publications are solely those of the individual author(s) and contributor(s) and not of MDPI and/or the editor(s). MDPI and/or the editor(s) disclaim responsibility for any injury to people or property resulting from any ideas, methods, instructions or products referred to in the content.